JACS
JOURNAL OF THE AMERICAN CHEMICAL SOCIETY
Article
pubs.acs.org/JACS

Understanding the Formation of Salt-Inclusion Phases: An Enhanced Flux Growth Method for the Targeted Synthesis of Salt-Inclusion Cesium Halide Uranyl Silicates

Gregory Morrison, Mark D. Smith, and Hans-Conrad zur Loye*

Department of Chemistry and Biochemistry, University of South Carolina, Columbia, South Carolina 29208, United States

Supporting Information

ABSTRACT: Salt-inclusion compounds (SICs) are known for their structural diversity and their potential applications, including luminescence and radioactive waste storage forms. Currently, the majority of salt-inclusion phases are grown serendipitously and the targeted growth of SICs has met with only moderate success. We report an enhanced flux growth method for the targeted growth of SICs. Specifically, the use of (1) metal halide reagents and (2) reactions with small surface area to volume ratios are found to favor the growth of salt-inclusion compounds over pure oxides and thus enable a more targeted synthetic route for their preparation. The Cs−X−U−Si−O (X = F, Cl) pentanary phase space is used as a model system to demonstrate the generality of this enhanced flux method approach. Single crystals of four new salt-inclusion uranyl silicates, $[Cs_3F][(UO_2)(Si_4O_{10})]$, $[Cs_2Cs_5F][(UO_2)_2(Si_6O_{17})]$, $[Cs_9Cs_6Cl][(UO_2)_7(Si_6O_{17})_2(Si_4O_{12})]$, and $[Cs_2Cs_5F][(UO_2)_3(Si_2O_7)_2]$, were grown using this enhanced flux growth method. A detailed discussion of the factors that favor salt-inclusion phases during synthesis and why specifically uranyl silicates make excellent frameworks for salt-inclusion phases is given.

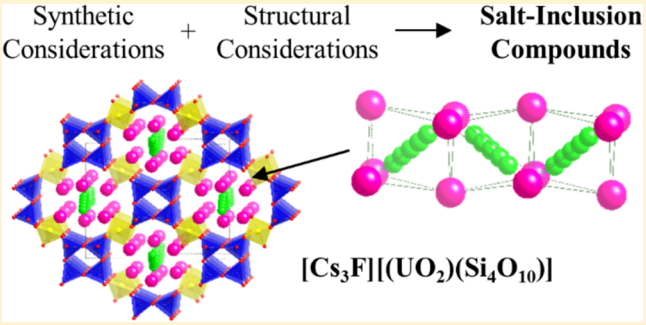

INTRODUCTION

Exploratory crystal growth is a vital aspect of solid-state chemistry, where the discovery of new compounds and structure types leads to new systems that can be optimized for a desired property and even to the discovery of new, unexpected properties. For much of its history, exploratory crystal growth has largely entailed targeting yet unexplored phase space. However, with the maturation of the field, the focus of this exploration has shifted toward the development of new synthesis methods that allow for the targeted growth of new compounds within already explored phase space. These new methods can be a brand new technique such as the modulated elemental reactants method[1] or can be a modification of an already used approach, such as the mild hydrothermal method for inorganic fluorides,[2−4] the two-step synthesis for reduced oxides,[5,6] or the recently developed hydroflux method.[7−9]

One class of materials that has garnered increasing attention is salt-inclusion phases, compounds which consist of a more covalent metal oxide framework containing voids filled by 0-D,[10,11] 1-D,[12−14] or 2-D[15] simple ionic salt lattices. Although salt-inclusion minerals have been known since the early 1900s,[16,17] during the past ∼15 years synthetic salt-inclusion phases have been recognized as an abundant and structurally diverse set of compounds.[18,19] Furthermore, they have received attention for their potential applications, such as for luminescence.[11] Interestingly, in the case of uranyl salt-inclusion compounds, these phases exhibit intense luminescence at room temperature, whereas in uranyl oxides the luminescence is typically thermally quenched.[20,21] Similar behavior has been observed for uranyl oxychlorides[22,23] and is likely due to the softening of the vibrational modes by the halide anion. Besides luminescence, many salt-inclusion phases are noncentrosymmetric, making them potential second harmonic generation materials.[12−14] Salt-inclusion compounds can also form porous materials,[18,24,25] can exhibit magnetic nanostructures,[19,26] and can have important applications as new waste forms for the safe, long-term storage of radioisotopes, such as Cs, I, Pu, and U.[27]

While of increasing interest, salt-inclusion compounds have remained a challenge to synthesize,[19,25] and most of the salt-inclusion phases that have been reported were grown serendipitously during the exploration of oxide systems.[11,28,29] These phases have predominately been grown from alkali halide fluxes but have also been grown from other salt fluxes,[30,31] such as $Na_2O−H_3BO_3$, and under hydrothermal conditions.[32,33] Some effort has been placed on the targeted growth of salt-inclusion compounds and, via the careful selection of systems and the use of mixed alkali halide eutectic fluxes, many new salt-inclusion phases have been prepared, often by resorting to intercalation of a salt-lattice into a known structure.[24]

Received: March 28, 2016
Published: May 24, 2016

DOI: 10.1021/jacs.6b03205
J. Am. Chem. Soc. 2016, 138, 7121−7129

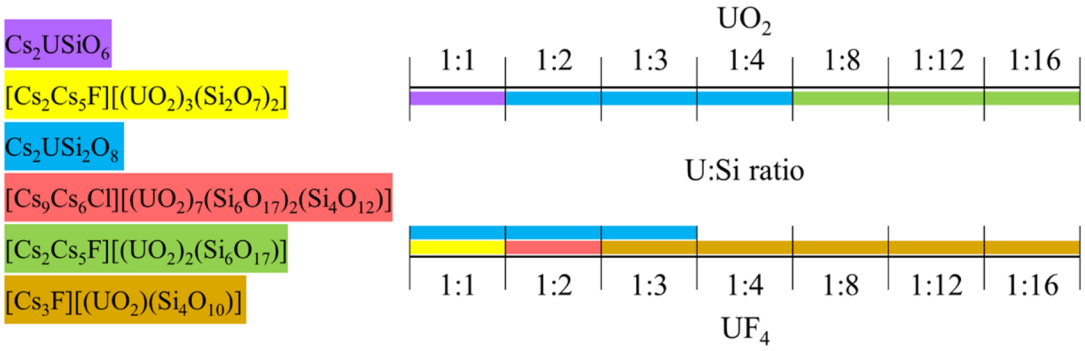

Figure 1. Uranyl silicate products of reactions with varying U:Si ratios using either UO_2 (top) or UF_4 (bottom) as the uranium source. Reaction products were determined by PXRD. All reactions also contained a large amount of AgCl which is not included in the figure.

Uranium silicates have been extensively studied as the abundance of silicon dioxide in the earth's crust leads to the formation of uranyl silicates in uranium deposits,[34] as well as when spent nuclear fuel interacts with the environment.[35,36] Silicates have also been investigated as potential waste storage media.[37] Currently, nuclear waste is predominately stored in glass form;[38] however, crystalline materials are being investigated as future storage media due to their enhanced water stability when compared to glasses.[39] Of particular interest are materials that can immobilize multiple constituents of spent nuclear fuel. In particular, cesium containing compounds are of interest as cesium is one of the most abundant fission products.[40,41] One class of materials that has been investigated are guest–host materials in which a covalent host uranyl framework accommodates an electrostatically bonded guest species, for example an alkali hydrate.[42] Salt-inclusion compounds have a similar structural motif making the investigation of salt-inclusion uranyl silicates of interest.

We have recently reported on the synthesis of two new salt-inclusion uranyl silicates, $[NaK_6F][(UO_2)_3(Si_2O_7)_2]$ and $[KK_6F][(UO_2)_3(Si_2O_7)_2]$.[27] In the case of $[NaK_6F]$-$[(UO_2)_3(Si_2O_7)_2]$ we found that the surface area to volume, sa/vol, ratio of the reaction had a strong influence on the reaction products, with small sa/vol ratios favoring the growth of salt-inclusion phases over pure oxides.[27] In this work, we discuss this enhancement to the flux growth method along with introducing a new enhancement, the use of halide as opposed to oxide precursors. We find that these two enhancements greatly favor the growth of salt-inclusion phases over pure oxides.

To articulate these enhancements, we will focus in this paper on the U(VI)–Si–O–CsCl/CsF phase space, in which to date we have discovered four new salt-inclusion phases, as well as our previously reported salt-inclusion compounds.[21,27] We find that while a subset of salt-inclusion phases can be grown using traditional flux growth techniques, a set which likely includes most of the serendipitously grown salt-inclusion phases, numerous other salt-inclusion phases require one or both of the enhancements discussed herein in order to be synthesized. To highlight this and to discuss the factors that favor salt-inclusion phases during synthesis, and why specifically uranium silicates make excellent frameworks for salt-inclusion phases, we present the synthesis and structure of the four new salt-inclusion cesium uranyl silicates, $[Cs_3F][(UO_2)(Si_4O_{10})]$ (**1**), $[Cs_2Cs_5F][(UO_2)_3(Si_2O_7)_2]$ (**2**), $[Cs_2Cs_5F][(UO_2)_2(Si_6O_{17})]$ (**3**), and $[Cs_9Cs_6Cl][(UO_2)_7(Si_6O_{17})_2(Si_4O_{12})]$ (**4**).

EXPERIMENTAL SECTION

Synthesis. U_3O_8 (International Bio-Analytical Industries, powder, ACS grade), UF_4 (International Bio-Analytical Industries, powder, ACS grade), CsF (Alfa Aesar, powder, 99%), and CsCl (Alfa Aesar, powder, 99%) were used as received. SiO_2 (Aldrich, fused pieces <4 mm, 99.99%) was ground in a ball mill and passed through a 250 μm sieve. UO_2 was prepared by heating U_3O_8 at 650 °C for 18 h. under a flow of 4% H_2 in N_2. ***Caution!*** *Although the uranium precursors used contain depleted uranium, standard safety measures for handling radioactive substances must be followed.*

For each reaction, a mixture of UF_4 or UO_2 and SiO_2 was placed in a silver crucible made from a 5.7 cm tall and 1.2 cm in diameter silver tube with a bottom welded on using a tungsten inert gas welder and covered with a mixture of 9 mmol CsF and 11 mmol CsCl. Specific reaction conditions to grow each compound are detailed in Figure 1. For reactions with a 1:4 U:Si ratio, 0.5 mmol of UF_4 or UO_2 and 2 mmol of SiO_2 were used. For reactions with a higher U content, the amount of SiO_2 was reduced and for reactions with a greater Si content, the amount of U precursor was reduced. In each case, the silver tube was loosely covered with a silver lid and placed in a programmable furnace. The reactions were heated to 800 °C in 1.5 h, dwelled at this temperature for 12 h, slow cooled to 400 °C at 6 °C/h, and then quickly cooled to room temperature by shutting off the furnace. The flux was removed via sonication in water and the reaction products were isolated via vacuum filtration.

$[Cs_3F][(UO_2)(Si_4O_{10})]$ (**1**) was grown using a UF_4:SiO_2 ratio of 1:4. This reaction yielded neon yellow-green rod crystals of $[Cs_3F][(UO_2)(Si_4O_{10})]$ (**1**), Figure 2, in ∼60% yield along with a large amount of polycrystalline AgCl. A phase pure sample of $[Cs_3F][(UO_2)(Si_4O_{10})]$ (**1**) was obtained via crystal picking.

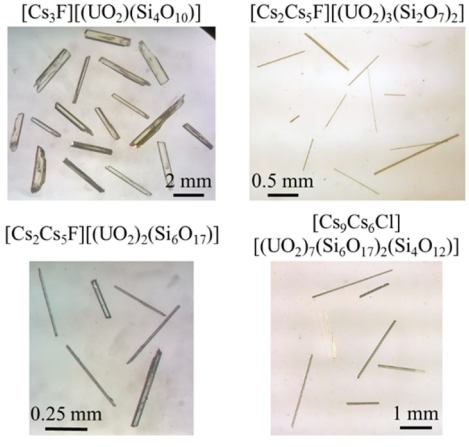

Figure 2. Single crystals of $[Cs_3F][(UO_2)(Si_4O_{10})]$ (**1**), $[Cs_2Cs_5F]$-$[(UO_2)_3(Si_2O_7)_2]$ (**2**), $[Cs_2Cs_5F][(UO_2)_2(Si_6O_{17})]$ (**3**), and $[Cs_9Cs_6Cl][(UO_2)_7(Si_6O_{17})_2(Si_4O_{12})]$ (**4**).

DOI: 10.1021/jacs.6b03205
J. Am. Chem. Soc. 2016, 138, 7121–7129

Table 1. Crystallographic Data for Cesium Halide Salt-Inclusion Uranyl Silicates

compound	$[Cs_3F][(UO_2)(Si_4O_{10})]$	$[Cs_2Cs_5F][(UO_2)_3(Si_2O_7)_2]$	$[Cs_2Cs_5F][(UO_2)_2(Si_6O_{17})]$	$[Cs_9Cs_6Cl][(UO_2)_7(Si_6O_{17})_2(Si_4O_{12})]$
space group	*Imma*	$P2_1/n$	$P2_12_12$	$P\bar{1}$
a (Å)	15.4758(4)	7.5564(5)	10.3741(3)	7.3497(2)
b (Å)	7.8147(2)	9.8644(7)	19.2795(7)	15.3322(5)
c (Å)	12.7559(4)	18.5543(13)	7.1800(2)	17.2547(5)
α (deg)	90	90	90	89.2960(10)
β (deg)	90	91.713(2)	90	89.9880(10)
γ (deg)	90	90	90	76.4460(10)
V (Å^3)	1542.68(7)	1382.41(17)	1436.05(8)	1890.08(10)
Z	4	2	2	1
crystal size (mm^3)	0.42 × 0.08 × 0.06	0.08 × 0.04 × 0.04	0.06 × 0.04 × 0.04	0.10 × 0.06 × 0.02
temperature (K)	301(2)	299(2)	304(2)	300(2)
density (g cm^{-3})	4.134	5.033	4.463	4.485
θ range (deg)	2.63−36.36	2.88−36.07	2.88−32.06	2.36−30.03
μ (mm^{-1})	17.871	26.860	20.341	22.453
Data Collection and Refinement				
collected reflections	40412	86130	84627	98100
unique reflections	2043	6677	5246	11075
R_{int}	0.0471	0.0374	0.0418	0.0377
h	$-23 \le h \le 25$	$-12 \le h \le 12$	$-15 \le h \le 15$	$-10 \le h \le 10$
k	$-13 \le k \le 13$	$-16 \le k \le 16$	$-29 \le k \le 29$	$-21 \le k \le 21$
l	$-21 \le l \le 21$	$-30 \le l \le 30$	$-10 \le l \le 10$	$-24 \le l \le 24$
$\Delta\rho_{max}$ (e Å^{-3})	3.527	3.998	3.646	6.632
$\Delta\rho_{min}$ (e Å^{-3})	−3.532	−3.163	−5.379	−5.792
GoF	1.126	1.217	1.170	1.142
extinction coefficient	0.00259(11)	0.00087(4)	n/a	n/a
$R_1(F)$ for $F_0^2 > 2\sigma(F_0^2)$[a]	0.0290	0.0383	0.0485	0.0548
$R_w(F_0^2)$[b]	0.0724	0.0864	0.1305	0.1215

[a] $R_1 = \Sigma||F_0| - |F_c||/\Sigma|F_0|$. [b] $wR_2 = [\Sigma w(F_0^2 - F_c^2)^2/\Sigma w(F_0^2)^2]^{1/2}$; $P = (F_0^2 + 2F_c^2)/3$; $w = 1/[\sigma^2(F_0^2) + (0.0300P)^2 + 24.5990P]$ for $[Cs_3F][(UO_2)(Si_4O_{10})]$, $w = 1/[\sigma^2(F_0^2) + (0.0134P)^2 + 32.1169P]$ for $[Cs_2Cs_5F][(UO_2)_3(Si_2O_7)_2]$, $w = 1/[\sigma^2(F_0^2) + (0.0498P)^2 + 32.1181P]$ for $[Cs_2Cs_5F][(UO_2)_2(Si_6O_{17})]$, and $w = 1/[\sigma^2(F_0^2) + (0.0194P)^2 + 104.1265]$ for $[Cs_9Cs_6Cl][(UO_2)_7(Si_6O_{17})_2(Si_4O_{12})]$.

$[Cs_2Cs_5F][(UO_2)_3(Si_2O_7)_2]$ (**2**) was grown using a UF_4:SiO_2 ratio of 1:1. This reaction yielded thin yellow needles of $[Cs_2Cs_5F][(UO_2)_3(Si_2O_7)_2]$ (**2**), Figure 2, in ∼10% yield along with large yellow crystals of $Cs_2USi_2O_8$, which have a similar morphology to $[Cs_3F][(UO_2)(Si_4O_{10})]$ (**1**), and a large amount of polycrystalline AgCl. $[Cs_2Cs_5F][(UO_2)_2(Si_6O_{17})]$ (**3**) was grown using a UO_2:SiO_2 ratio of 1:8. This reaction yielded small yellow rod crystals of $[Cs_2Cs_5F][(UO_2)_2(Si_6O_{17})]$ (**3**), Figure 2, in ∼10% yield along with a large amount of polycrystalline AgCl. $[Cs_9Cs_6Cl][(UO_2)_7(Si_6O_{17})_2(Si_4O_{12})]$ (**4**) was grown using a UF_4:SiO_2 ratio of 1:2. This reaction yielded yellow rods of $[Cs_9Cs_6Cl][(UO_2)_7(Si_6O_{17})_2(Si_4O_{12})]$ (**4**), Figure 2, in ∼20% yield along with large yellow crystals of $Cs_2USi_2O_8$ and a large amount of polycrystalline AgCl.

Structure. Single crystal X-ray diffraction, SXRD, data for each compound were collected on a Bruker D8 QUEST diffractometer equipped with an Incoatec microfocus Mo Kα source (λ = 0.71073 Å) and a PHOTON 100 CMOS area detector. Diffraction data were processed using SAINT+[43] and corrected for absorption effects with a multiscan absorption correction using SADABS.[44] ShelXT[45] was used to obtain an initial structure solution via direct methods which was then refined using ShelXL[46] in the OLEX2[47] and WinGX[48] interfaces. Crystallographic data for each compound are provided in Table 1.

Structure determination using SXRD data was challenging due to the strong absorbing nature of both U and Cs and by the low dimensionality of the crystals of each compound. To obtain the best quality data possible, a high redundancy of data (redundancy >9 for most reflections), was collected to improve the multiscan absorption correction. Structure determination was further complicated by the presence of disorder in the salt-inclusion of each reported compound and by the presence of twinning in $[Cs_2Cs_5F][(UO_2)_2(Si_6O_{17})]$ (**3**) (inversion twin), and $[Cs_9Cs_6Cl][(UO_2)_7(Si_6O_{17})_2(Si_4O_{12})]$ (**4**) (pseudomerohedral twin). In each case, the model presented here yielded a physically sensible structure and the best refinement statistics. The higher R-values and less smooth residual electron density maps obtained from these refinements (in comparison with typical SXRD solutions) are a direct result of strongly absorbing, disordered, nonideal crystals and not the result of incorrect structure solutions. It is also important to note that in all cases, the largest residual electron density maxima are less than 10% of the electron density of the adjacent heavy atoms.

$[Cs_3F][(UO_2)(Si_4O_{10})]$ (**1**) crystallizes in the orthorhombic space group *Imma* and refined to R_1 = 0.0290 with a reasonably flat final difference map. The largest residual electron density peak and hole, 3.527 and −3.532 e$^-$/Å^3, are located 0.63 and 0.28 Å from Cs(2), respectively. Disorder was observed on the F site. When only one F site was modeled, a highly prolate atomic displacement parameter, U_3/U_1 = 45.5, was observed. This disorder was modeled as five F positions (F1, F(2) × 2, and F(3) × 2) with a total occupancy of 1. $[Cs_2Cs_5F][(UO_2)_3(Si_2O_7)_2]$ (**2**) crystallizes in the monoclinic space group $P2_1/n$ and refined to R_1 = 0.0383. The largest residual electron density peak of 3.998 e$^-$/Å^3 is located 0.90 Å from U(1) and hole of −3.163 e$^-$/Å^3 is located 1.468 Å from O(3) and ∼1.82 Å from the split Cs(4) sites. Both the F(1) and Cs(4) atoms are split across an inversion center. When no atom is modeled on either site, two residual electron density peaks are observed. $[Cs_2Cs_5F][(UO_2)_2(Si_6O_{17})]$ (**3**) crystallizes in the orthorhombic space group $P2_12_12$ and refined to R_1 = 0.0485. The largest residual electron density peak of 3.646 e$^-$/Å^3 is located 1.76 Å from Cs(2) and hole of −5.379 e$^-$/Å^3 is located 1.92 Å from Cs(1). Disorder was observed in the Cs(4) site. When only one site was modeled a very prolate atomic displacement parameter, U_3/U_1 = 7.5, and a large residual electron density peak, 5.11 e$^-$/Å^3, on one side of the site were observed. This disorder was modeled as a main Cs(4a) site with an occupancy of 92.8(5) % and a Cs(4b) site with an

DOI: 10.1021/jacs.6b03205
J. Am. Chem. Soc. 2016, 138, 7121−7129

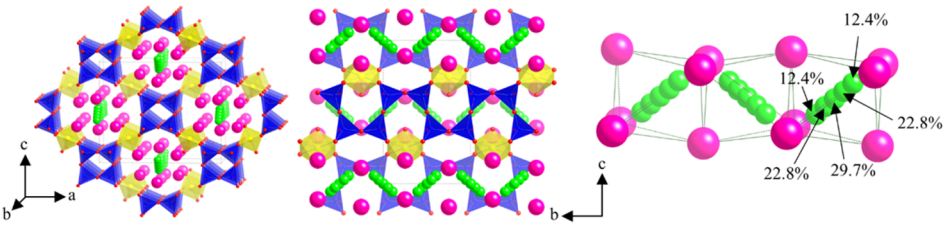

Figure 3. Structure of $[Cs_3F][(UO_2)(Si_4O_{10})]$ (**1**) showing the view down the *b*-direction (left), the view down the *a*-direction (center), and the salt-inclusion (right). Silicate polyhedra are shown in blue, uranium polyhedra in yellow, cesium atoms in pink, and fluorine atoms in green, and oxygen atoms in red.

occupancy of 7.2(5) %. When the atomic displacement parameter for O(8) was freely anisotropically refined an unreasonably flat ellipsoid was observed, likely due to its proximity to the disordered Cs(4) sites. For this reason, the displacement parameters for O(8) were refined using an ISOR command with σ = 0.005. $[Cs_9Cs_6Cl][(UO_2)_7(Si_6O_{17})_2(Si_4O_{12})]$ (**4**) crystallizes in the triclinic space group $P\bar{1}$ and refined to R_1 = 0.0548. The largest residual electron density peak of 6.637 $e^-/Å^3$ is located 0.73 Å from U(2) and hole of −5.779 $e^-/Å^3$ is located 0.59 Å from U(3). A large amount of Cs disorder was observed in one region of the structure. When no Cs atoms were modeled in this region, eight residual density peaks were observed around an inversion center. When modeled as partially occupied Cs atoms, the occupancies freely refined to a total occupancy of 3.03. To charge balance, the total occupancy of these eight sites was constrained to 3 using a SUMP command.

Powder X-ray diffraction, PXRD, data was collected on bulk portions of each reaction product. Data was collected on a Rigaku Ultima IV diffractometer with a Cu Kα source (λ = 1.54056 Å) and a D/teX detector. The diffraction patterns, Figure S1, were used to identify the products of each reaction. PXRD data was also used to confirm the purity of the picked $[Cs_3F][(UO_2)(Si_4O_{10})]$ (**1**) sample, Figure S2. Energy dispersive spectroscopy data on single crystals of each compound were collected on a TESCAN Vega-3 SBU equipped with an EDS detector. Qualitatively, elemental analysis using this data confirmed the presence of Cs, U, Si, O, and the expected halide in each compound and, within the detection limits of the instrument, confirmed the absence of Ag and the other halide.

Fluorescence. Fluorescence data for $[Cs_3F][(UO_2)(Si_4O_{10})]$ (**1**) were collected on a PerkinElmer LS55 Luminescence Spectrometer. Excitation data were collected at an emission wavelength of 545 nm and emission data were collected at an excitation wavelength of 411 nm.

RESULTS AND DISCUSSION

Synthesis. Alkali halide fluxes, especially mixed alkali halides, are a versatile flux for the synthesis of oxides, as they are capable dissolving most metal oxide starting materials.[49] In some instances, the use of alkali halide fluxes can lead to the growth of salt-inclusion phases. Historically, such phases were grown serendipitously, although the growth of salt-inclusion phases can be made more likely by careful selection of system and precursors. We have recently reported that decreasing the surface area to volume, sa/vol, ratio of the reaction can greatly increase the likelihood of producing a salt-inclusion phase.[27] This is believed to be due to the decreased availability of atmospheric oxygen to the reaction favoring the inclusion of other anions in the product. We have observed that some salt-inclusion phases are highly dependent on the sa/vol ratio while others readily grow even in reactions with a very high sa/vol ratio. For example, $[NaK_6F][(UO_2)_3(Si_2O_7)_2]$ could only be grown in the tall silver tube based crucible described in the experimental section, whereas $[KK_6Cl][(UO_2)_3(Si_2O_7)_2]$ readily grows even in a shallowly filled 75 mL silver crucible.[27] Similarly, $[Cs_3F][(UO_2)(Si_4O_{10})]$ (**1**) could only be grown using the silver tube based crucible. If the same reaction was carried out in a 14 mL high form or 75 mL conical crucible the major products were $Cs_2USi_2O_8$ and AgCl, with no $[Cs_3F][(UO_2)(Si_4O_{10})]$ (**1**). The reaction was also performed in a 24 mL high form Pt crucible and yielded similar products to the 14 mL Ag crucible reaction except without the formation of AgCl, suggesting that the formation of AgCl does not affect the other reaction products.

As discussed above, the competition between the growth of salt-inclusion phases versus pure oxides appears to be very dependent on the availability of oxide versus halide ions in the melt. It follows that the use of metal halide reagents instead of metal oxide reagents may favor the growth of salt-inclusion phases. Indeed, this is found to be the case for $[Cs_3F][(UO_2)(Si_4O_{10})]$ (**1**), $[Cs_2Cs_5F][(UO_2)_3(Si_2O_7)_2]$ (**2**), and $[Cs_9Cs_6Cl][(UO_2)_7(Si_6O_{17})_2(Si_4O_{12})]$ (**4**), which can only be grown when a uranium fluoride, UF_4 or UF_3, is used as the uranium source. In the case of $[Cs_3F][(UO_2)(Si_4O_{10})]$ (**1**), when either UO_2 or U_3O_8 are used, $Cs_2USi_2O_8$ is formed instead. On the other hand, $[Cs_2Cs_5F][(UO_2)_2(Si_6O_{17})]$ (**3**), only formed when a uranium oxide precursor was used. This may be because $[Cs_3F][(UO_2)(Si_4O_{10})]$ (**1**) readily grows under the same conditions when a uranium fluoride precursor is used, kinetically preventing the growth of $[Cs_2Cs_5F][(UO_2)_2(Si_6O_{17})]$ (**3**).

We have observed two possible results when a uranium fluoride is used instead of a uranium oxide. In some cases, such as the $[Cs_3F][(UO_2)(Si_4O_{10})]$ (**1**) reaction, a different product is observed when UF_4 is used. Similarly, when UF_4 is substituted for U_3O_8 in our reported growth of $[NaK_6F][(UO_2)_3(Si_2O_7)_2]$,[27] a different salt-inclusion phase, $K_8(K_5F)U_6Si_8O_{40}$,[21] is formed. In other cases, the use of UF_4 instead leads to the growth of larger crystals of the same product as is grown using U_3O_8. For example, in the targeted growth of $K_8(K_5F)U_6Si_8O_{40}$, the use of UF_4 produced larger crystals than the same growth with U_3O_8.[21]

Structure. All four compounds consist of a uranyl silicate framework that contains voids in which the salt-inclusion is located. In each compound, the uranium atoms adopt a typical uranyl geometry[50] with two short axial U−O bonds, 1.777(13)−1.891(12) Å and four longer equatorial U−O bonds, 2.207(14)-2.281(12) Å. Likewise, the silicon atoms adopt the typical tetrahedral silicate geometry[51] with bond distances of 1.570(15)−1.656(12) Å. Specific bond distances, along with bond valence sums,[52,53] for each compound are listed in Tables S1−S4. The structural formula $[A_mB_nX][(UO_2)_p(Si_qO_r)_t]$ is used throughout this manuscript, where $[(UO_2)_p(Si_qO_r)_t]$ is the framework consisting of uranyl, UO_2^{2+}, units and Si_qO_r units, B_nX is the salt-inclusion and A are alkali cations which are not part of the salt-inclusion.

DOI: 10.1021/jacs.6b03205
J. Am. Chem. Soc. 2016, 138, 7121−7129

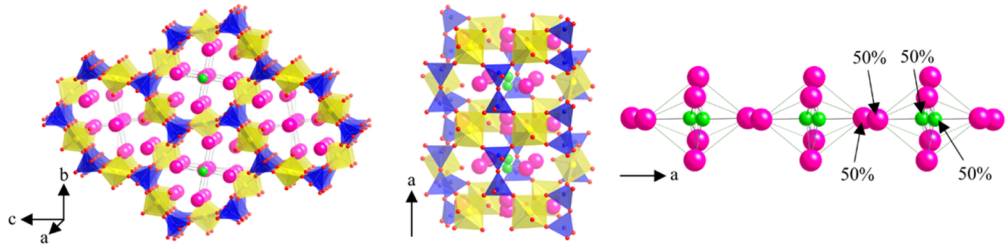

Figure 4. Structure of $[Cs_2Cs_5F][(UO_2)_3(Si_2O_7)_2]$ (**2**) showing the view down the *a*-direction (left), the channel created by the 12-member ring (center), and the salt-inclusion (right). Silicate polyhedra are shown in blue, uranium polyhedra in yellow, cesium atoms in pink, and fluorine atoms in green, and oxygen atoms in red.

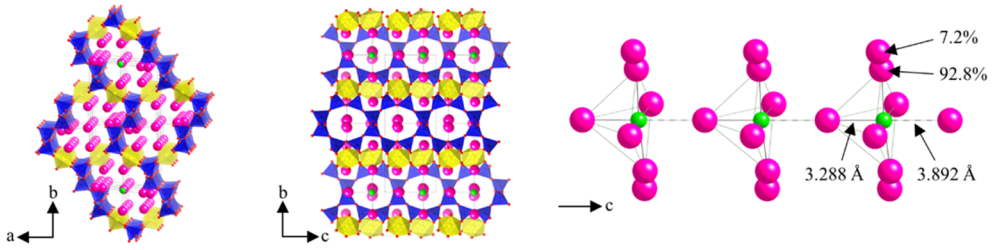

Figure 5. Structure of $[Cs_2Cs_5F][(UO_2)_2(Si_6O_{17})]$ (**3**) showing the view down the *c*-direction (left), the view down the *a*-direction (center), and the salt-inclusion (right). Silicate polyhedra are shown in blue, uranium polyhedra in yellow, cesium atoms in pink, and fluorine atoms in green, and oxygen atoms in red.

$[Cs_3F][(UO_2)(Si_4O_{10})]$ (**1**), shown in Figure 3, crystallizes in the orthorhombic space group *Imma* with lattice parameters a = 15.4758(4) Å, b = 7.8147(2) Å, and c = 12.7559(4) Å. The asymmetric unit of the structure consists of one U site, one Si site, two Cs sites, five O sites and three disordered F sites. The silicate tetrahedra form Si_4O_{10} columns in the *b*-direction. These columns are connected in the *a*- and *c*-directions by isolated UO_6 polyhedra to form 12 member uranyl silicate rings (U−Si−Si−U−Si−Si−U−Si−Si−U−Si−Si). The Cs_3F salt inclusion is located in the center of these rings and can be described as columns of face sharing Cs_6F octahedra, where significant disorder exists in the position of the fluorine anion about a 2-fold axes of the Cs_6F octahedron. This disorder was modeled as a central F(1) surrounded by a F(2) and F(3) on each side with occupancies 0.30, 0.23, and 0.12, respectively.

$[Cs_2Cs_5F][(UO_2)_3(Si_2O_7)_2]$ (**2**), shown in Figure 4, crystallizes in the monoclinic space group $P2_1/n$ with lattice parameters a = 7.5564(5) Å, b = 9.8644(7) Å, c = 18.5543(13) Å, and β = 91.713(2)°. The asymmetric unit consists of two U sites, two Si sites, three ordered and one disordered Cs site, ten O sites and one disordered F site. The structure is related to the structures of the previously reported $[AB_6X][(UO_2)_3(Si_2O_7)_2]$ ($[AB_6X]$ = $[NaRb_6F]$, $[NaK_6F]$, or $[KK_6Cl]$) and $[KK_2Cs_4F][(UO_2)_3(Si_2O_7)_2]$, reported as $[K_3Cs_4F][(UO_2)_3(Si_2O_7)_2]$, which crystallize in the space groups *Pnnm* and $Cmc2_1$, respectively.[27,28] $[Cs_2Cs_5F][(UO_2)_3(Si_2O_7)_2]$ (**2**) contains the same uranyl silicate framework as the $[AB_6X][(UO_2)_3(Si_2O_7)_2]$ compounds, although the framework is slightly monoclinically distorted, likely due to the large size of the Cs cations compared to the other alkali cations. This framework, which is described in more detail elsewhere,[27,28] is made up of isolated uranium polyhedra that corner share with Si_2O_7 units to form 12 member uranyl silicate rings (U−Si−U−Si−U−Si−U−Si−U−Si−U−Si). $[Cs_2Cs_5F][(UO_2)_3(Si_2O_7)_2]$ (**2**) differs from the other $[AB_6X][(UO_2)_3(Si_2O_7)_2]$ compounds in the location and identity of the $[A_nB_mX]$ unit. The other compounds all contain a single small A cation, Na^+ or K^+, which is located in the center of a U−Si−Si−U−Si−Si ring within the uranyl silicate framework. Cs^+ is too large to fit into this site and instead shifts to either side of the ring, doubling the A cation occupancy. At the same time, the salt-inclusion, which are isolated B_6X units in the other compounds, rotate to become corner sharing. Disorder in the F and shared Cs sites lead to the actual salt-inclusion being isolated Cs_5F units with a sixth longer Cs−F bond.

$[Cs_2Cs_5F][(UO_2)_2(Si_6O_{17})]$ (**3**), shown in Figure 5 and Figure S3, crystallizes in the orthorhombic space group $P2_12_12$ with lattice parameters a = 10.3741(3) Å, b = 19.2795(7) Å, and c = 7.1800(2) Å. The asymmetric unit consists of one U site, three Si sites, three ordered and one disordered Cs site, 11 O sites and one F site. The silicate tetrahedra corner share to form Si_6O_{17} chains. These chains can be viewed as individual 8-member silicate rings which share two silicate units with each of the adjacent rings. The four nonshared silicate units within the 8-member ring exist as two pairs, each of which corner shares one oxygen each with two uranyl polyhedra and two oxygens with a third uranyl polyhedron, Figure S3. This creates 14 member uranyl silicate rings (U−Si−Si−Si−Si−U−Si−U−Si−Si−Si−Si−U−Si) that form channels down the *c*-direction. Both the B_5X salt-inclusion and the A cations are located in these channels and have an arrangement similar to that found for the $[Cs_2Cs_5F]$ units in $[Cs_2Cs_5F][(UO_2)_3(Si_2O_7)_2]$ (**2**). Specifically, the Cs_5F salt-inclusions form pseudo corner-sharing Cs_6F octahedra, where the shared Cs atoms are shifted toward one F atom, Cs−F = 3.288 Å, to form Cs_5F square pyramids with a sixth longer Cs−F bond, Cs−F = 3.892 Å, and the two nonsalt-inclusion Cs cations lie between four equatorial salt-inclusion Cs atoms and are on opposite sides of the salt-inclusion. Unlike in $[Cs_2Cs_5F][(UO_2)_3(Si_2O_7)_2]$ (**2**), in $[Cs_2Cs_5F][(UO_2)_2(Si_6O_{17})]$ (**3**) the F and shared Cs atoms in the salt-inclusion are completely ordered, and instead, two of the equatorial Cs atoms, both Cs(4) atoms, are disordered where the Cs(4A) atoms, occupancy = 92.8(5) %, are within bonding range of the central F atom, Cs−F = 3.166 Å, and the

DOI: 10.1021/jacs.6b03205
J. Am. Chem. Soc. 2016, 138, 7121−7129

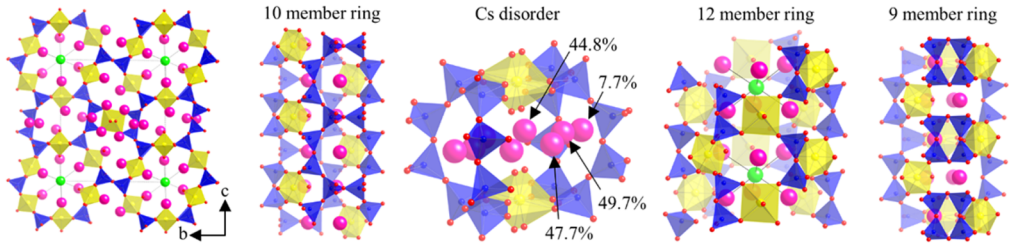

Figure 6. Structure of $[Cs_9Cs_6Cl][(UO_2)_7(Si_6O_{17})_2(Si_4O_{12})]$ (**4**) showing, from left to right, the view down the *a*-axis, the channel created by the 10-member ring, the environment around the disordered Cs sites, the channel created by the 12-member ring, and the channel created by the 9-member ring. Silicate polyhedra are shown in blue, uranium polyhedra in yellow, cesium atoms in pink, and fluorine atoms in green, and oxygen atoms in red.

Cs(4B) atoms, occupancy = 7.2(5) %, are outside of the bonding range, Cs−F = 4.227 Å.

$[Cs_9Cs_6Cl][(UO_2)_7(Si_6O_{17})_2(Si_4O_{12})]$ (**4**), shown in Figure 6, crystallizes in the triclinic space group $P\bar{1}$ with lattice parameters a = 7.3497(2) Å, b = 15.3322(5) Å, c = 17.2547(5) Å, α = 89.2960(10)°, β = 89.9880(10)°, and γ = 76.4460(10)°. The asymmetric unit consists of four U sites, eight Si sites, six ordered and four disordered Cs sites, twenty-eight ordered and six disordered O sites and one Cl site. Unlike in the other reported compounds, the silicate tetrahedra form two types of silicate motifs, Si_6O_{17} chains and Si_4O_{12} squares, within the structure. This is the second example of a uranyl silicate with more than one silicate motif, the first being $K_8(K_5F)U_6Si_8O_{40}$.[21] In $[Cs_9Cs_6Cl][(UO_2)_7(Si_6O_{17})_2(Si_4O_{12})]$ (**4**), two Si_6O_{17} chains corner share with U(1) polyhedra to form 10 member rings (U−Si−Si−Si−Si−U−Si−Si−Si−Si) that create channels in the *a* direction. Each U(1) polyhedron corner shares with two silicate units of each silicate chain; however due to the alignment of the U(1) polyhedra on either side of the channel, both of these silicate units are from the same 8 member silicate ring (recall that Si_6O_{17} chains are composed of 8 member silicate rings that share two silicate units with each adjacent ring) on one side and from two different 8 member silicate rings on the other. The 10 member rings are connected to each other in the *b*-direction by U(4) polyhedra to create $(U(1)O_2)_2(Si_6O_{17})_2U(4)O_2$ slabs in the *ab* plane. The Si_4O_{12} squares share two corners each with two U(2) polyhedra which lie on opposite sides of the square. These $(U(2)O_2)_2(Si_4O_{12})$ units are connected to each other in the *a*-direction by corner sharing with two U(3) polyhedra on either side to form $(U(2)O_2)_2(Si_4O_{12})(U(3)O_2)_2$ columns. The $(U(2)O_2)_2(Si_4O_{12})(U(3)O_2)_2$ columns corner share with the Si_6O_{17} chains of the $(U(1)O_2)_2(Si_6O_{17})_2U(4)O_2$ slab to form the 3-D uranyl silicate framework. This creates 9 member (U−Si−Si−U−Si−Si−U−Si−Si) and 12 member (U−Si−U−Si−U−Si−U−Si−U−Si−U−Si) uranyl silicate rings which form channels in the *a*-direction.

In $[Cs_9Cs_6Cl][(UO_2)_7(Si_6O_{17})_2(Si_4O_{12})]$ (**4**), the salt-inclusion, isolated Cs_6Cl octahedra, are located in the channels created by the 12 member uranyl silicate ring. The other two channels are both occupied by nonsalt-inclusion Cs atoms. Finally, the connection of the 10 member rings by U(4) polyhedra creates $(Si_8O_{24})_2U(4)_2$ cages which are occupied by eight disordered Cs atoms that sum to a total occupancy of three. Likely due to this disorder, the $U(4)O_6$ polyhedra are disordered over an inversion center such that the $U(4)O_6$ polyhedra are tilted one direction 50% of the time and tilted the other direction the remaining time.

Salt-Inclusions. As has been discussed in prior work,[27] salt-inclusion structures are very suitable for uranyl compounds. The two short uranyl oxygens have little tendency to bond further and, when they do, it is typically with low valent cations.[22,54] In salt-inclusion phases, these special bonding requirements can be accommodated for in a three-dimensional structure by having the uranyl oxygens point into the salt-inclusion. This is the case in all of the reported compounds, where the uranyl silicate rings are formed by the equatorial UO_6 oxygens and where the axial uranyl oxygens point into the salt-inclusion channels.

Along with salt-inclusion structures being suitable for uranyl compounds, uranyl silicates appear to be very suitable for salt-inclusions. Empirically, this can be seen by the large number and variety of salt-inclusion uranyl silicates.[21,27,28,32] There are two aspects of uranyl silicates which likely make them suitable for salt-inclusions. First, the bonding environment in uranyl silicates makes them more suitable to form salt-inclusion phases than oxyanion phases. The two main types of mixed anion oxides are the salt-inclusion phases, where the nonoxygen anion is located in a salt-lattice, and the oxyanion phases, where the nonoxygen anion is located in a MO_xX_y polyhedron (M = multivalent cation). In most uranyl silicates, every oxygen is either a uranyl, UO_2^{2+}, oxygen or a silicate oxygen. Each U-Oyl bond (Oyl = uranyl oxygen) has a bond valence of roughly two, which cannot be fulfilled by a halide ion. At the same time, the Si−O bond is very strong, 799(13) kJ/mol,[55] making it unlikely to be replaced by a halide ion and, in fact, crystalline compounds containing $[SiO_xF_y]$ species are not yet known.[56] For these reasons, uranyl silicate oxyhalides are unlikely to exist, favoring the formation of salt-inclusion silicates. The enhanced flux growth technique reported here appears to increase the likelihood of a mixed anion compound forming. In the uranyl silicates, this results predominantly in salt-inclusion phases, whereas is other systems, such as the lanthanide silicates, this often results in oxyhalides.

Second, uranyl silicates are suitable for salt-inclusions because of their ability to be charge balanced by salt-inclusions. In a simplistic view, most oxides can be viewed as an anionic framework that is charge balanced by low valent cations, often alkali or alkaline earth cations. In a salt-inclusion phase, part or all of the charge balancing is accomplished by the presence of the salt-inclusion. However, a salt-inclusion is much less charge dense than alkali or alkaline earth cations ($Cs^+ \approx 24$ Å^3/positive charge compared to $Cs_6F \approx 56$ Å^3/positive charge).[55,57−59] Therefore, for a salt-inclusion phase to exist, the framework must be able to form a large void that can accommodate the large salt-inclusion species, while at the same time not being so highly negatively charged that the salt-inclusion is unable to

DOI: 10.1021/jacs.6b03205
J. Am. Chem. Soc. 2016, 138, 7121−7129

Table 2. Summary of Framework Charge and Contents for Each Channel within the Cesium Halide Salt-Inclusion Uranyl Silicates

		per channel·(unit cell)											
compound	channel	U	charge/U	portion of charge to this channel[a]	Si	charge/Si[b]	portion of charge to this channel[a]	total charge of channel framework	channel size[c] (Å^3)	A cations	B_nX salt-inclusion	total charge of cations	cation inverse charge density (Å^3/positive charge)
$[Cs_3F][(UO_2)(Si_4O_{10})]$ (**1**)	12-member U–Si–Si–U–Si–Si–U–Si–Si–U–Si–Si	4	+2	1/2	16	−1	1/2	−4	290	–	Cs_3F ×2	+4	72.5
$[Cs_2Cs_5F][(UO_2)_3(Si_2O_7)_2]$ (**2**)	12-member U–Si–U–Si–U–Si–U–Si–U–Si–U–Si	6	+2	1/2	12	−3	1/3	−6	283.05	Cs ×2	Cs_5F	+6	47.2
$[Cs_2Cs_5F][(UO_2)_2(Si_6O_{17})]$ (**3**)	14-member U–Si–Si–Si–Si–U–Si–U–Si–Si–Si–Si–U–Si	4	+2	1/2	4 12	−5/3 −5/3	1/3 1/2	−6	291.75	Cs ×2	Cs_5F	+6	48.6
	12-member U–Si–U–Si–U–Si–U–Si–U–Si–U–Si	6	+2	1/2	4 8	−2 −5/3	1/3 1/3	−1.111	295.4	–	Cs_6Cl	+5	59.1
$[Cs_9Cs_6Cl][(UO_2)_7(Si_6O_{17})_2(Si_4O_{12})]$ (**4**)	10-member U–Si–Si–Si–Si–U–Si–Si–Si–Si	2	+2	1/2	8 4	−5/3 −5/3	1/3 1/2	−5.777	135.6	Cs ×3.164	–	+3.164	42.9
	9-member U–Si–Si–U–Si–Si–U–Si–Si	3	+2	1/2	2 4 4	−5/3 −5/3 −2	1/2 1/3 1/3	−3.555	112.6	Cs ×2.933	–	+2.933	38.4

[a]Charge is treated as distributed equally between each channel of which the polyhedron is a member. [b]Charge per Si for each silicate motif are as follows: Si_2O_7 = −3/Si, Si_4O_{12} = −2/Si, Si_6O_{17} = −1.66/Si, Si_4O_{10} = −1/Si [c]Channel size was determined by deleting all occupants of the channel in the CIF and then using the Calc Solv functionality in Platon[61] which calculates the solvent accessible volume

J. Am. Chem. Soc. 2016, 138, 7121−7129 DOI: 10.1021/jacs.6b03205

provide charge compensation in the available void space, i.e., the framework cannot be highly anionic. In a uranyl silicate, the silicate contributes −4 or less charge per silicon depending on the extent of the silicate condensation. An isolated SiO_4 tetrahedron contributes a charge of −4/Si to the framework while the silicate units in the reported structures, Si_2O_7, Si_4O_{12}, Si_6O_{17}, and Si_4O_{10}, contribute charges of −3/Si, −2/Si, −1.66/Si, and −1/Si, respectively. At the same time the uranyl contributes a + 2 charge to the framework. This enables the uranyl silicate framework to create large void spaces to accommodate the salt-inclusion, while maintaining a sufficiently low framework charge that the salt-inclusion can charge compensate. This also explains why $[Cs_3F][(UO_2)(Si_4O_{10})]$ (**1**), with the least charge dense silicate unit, −1/Si, is completely charge balanced by its salt-inclusion, whereas the other three reported compounds, with charges of −3/Si, −1.75/Si, and −1.66/Si, require, in addition to the salt-inclusion, nonsalt inclusion Cs cations to achieve charge balance.

Table 2 examines the specific channels within each cesium halide salt-inclusion uranyl silicate. As an example, $[Cs_3F][(UO_2)(Si_4O_{10})]$ (**1**) contains one type of channel formed by a 12 member U−Si−Si−U−Si−Si−U−Si−Si−U−Si−Si ring. This channel is composed of 4 U and 16 Si polyhedra per unit cell. Each uranyl unit has a charge of +2 and each Si tetrahedron has a charge of −1 (charge density of Si_4O_{10} = −1/Si). However, every polyhedron is shared by two channels. Assuming that the charge is shared equally between the channels, this means that the uranyl silicate framework has a charge density of −4/channel·(unit cell). Inside the channel, which has a volume of 290 $Å^3$/unit cell, are located two face sharing Cs_6F polyhedra, i.e., Cs_3F ×2. This salt-inclusion generates the requisite positive charge, + 4/channel·(unit cell), required to compensate the negative charge amassed in the formation of the channel framework. On the basis of the channel volume and cationic charge of its occupants, the salt-inclusion has an inverse charge density of 72.5 $Å^3$/positive charge.

As expected, Table 2 shows that the salt-inclusions have a lower charge density than the nonsalt-inclusion Cs atoms. The two channels containing only a salt-inclusion have the lowest charge density whereas the two channels containing only nonsalt-inclusion Cs atoms have the highest charge density. Finally, the two channels containing both have an intermediate charge density. Interestingly, all four salt-inclusion containing channels have approximately the same volume. This suggests that any of the observed channel occupants, $[Cs_3F]_2$, $[Cs_2Cs_5F]$, and $[Cs_6Cl]$, could fit in each channel and that the identity of the channel occupants is dictated by the requisite cationic charge.

Fluorescence. The luminescence of $[Cs_3F][(UO_2)(Si_4O_{10})]$ is shown in Figure 7. Similar to our other reported salt-inclusion uranyl silicates,[21,27] $[Cs_3F][(UO_2)(Si_4O_{10})]$ exhibits intense luminescence at room temperature. The luminescence has the typical color and peaks of the UO_2^{2+} unit.[34,60] The emission spectrum, excited at 411 nm, has five distinct peaks at 525, 545, 567, 591, and 619 nm. These emission peaks are the result of relaxation from the first excited electronic state coupled with different symmetric stretching modes of the uranyl.[34]

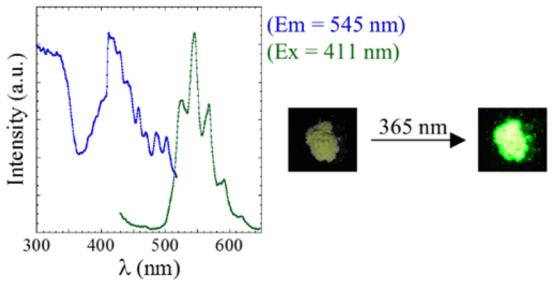

Figure 7. Luminescence of $[Cs_3F][(UO_2)(Si_4O_{10})]$ (**1**) along with pictures of the ground sample under artificial and UV-light (bottom).

CONCLUSION

The competition between the formation of salt-inclusion phases and regular oxides appears to be highly dependent on the relative availability of oxygen versus other anions in the synthetic melt environment. The reduction of the surface area to volume ratio of the melt, coupled with the use of metal halide precursors, creates synthetic conditions that strongly favor the formation of salt-inclusion compounds, SICs, over regular oxides. For example, the synthesis of $[Cs_3F][(UO_2)(Si_4O_{10})]$ (**1**) can only be achieved by using a uranium fluoride precursor, UF_4 or UF_3, and by performing the reaction in a tall, narrow silver tube crucible, which limits the availability of atmospheric oxygen in the melt.

Salt-inclusion phases have become of increasing interest due to their structural diversity and potential applications. However, the vast majority of salt-inclusion phases are still discovered serendipitously. Our research suggests that these serendipitously discovered salt-inclusion phases, which are typically grown under traditional flux growth conditions, represent only a subset of SICs, while many other salt-inclusion phases can be prepared by optimizing the melt reaction environment to favor SICs. The reported enhanced flux growth technique therefore represents an exciting new method that offers the potential for the discovery of numerous new salt-inclusion compounds and structure types.

ASSOCIATED CONTENT

Supporting Information

The Supporting Information is available free of charge on the ACS Publications website at DOI: 10.1021/jacs.6b03205.

Select interatomic distances and bond valence sums for $[Cs_3F][(UO_2)(Si_4O_{10})]$ (**1**), $[Cs_2Cs_5F][(UO_2)_3(Si_2O_7)_2]$ (**2**), $[Cs_2Cs_5F][(UO_2)_2(Si_6O_{17})]$ (**3**), and $[Cs_9Cs_6Cl][(UO_2)_7(Si_6O_{17})_2(Si_4O_{12})]$ (**4**). Powder X-ray diffraction data for each reaction shown in Figure 1 and for $[Cs_3F][(UO_2)(Si_4O_{10})]$ (**1**). Classification of all uranyl silicates based their silicate, uranium, and overall dimensionality. (PDF)

Single-crystal X-ray diffraction CIFs for $[Cs_3F][(UO_2)(Si_4O_{10})]$ (**1**), $[Cs_2Cs_5F][(UO_2)_3(Si_2O_7)_2]$ (**2**), $[Cs_2Cs_5F][(UO_2)_2(Si_6O_{17})]$ (**3**), and $[Cs_9Cs_6Cl][(UO_2)_7(Si_6O_{17})_2(Si_4O_{12})]$ (**4**). (CIF)

AUTHOR INFORMATION

Corresponding Author

*zurLoye@mailbox.sc.edu

Notes

The authors declare no competing financial interest.

DOI: 10.1021/jacs.6b03205
J. Am. Chem. Soc. 2016, 138, 7121−7129

■ ACKNOWLEDGMENTS

Research supported by the U.S. Department of Energy, Office of Basic Energy Sciences, Division of Materials Sciences and Engineering under Award DE-SC0008664.

■ REFERENCES

(1) Johnson, D. C. *Curr. Opin. Solid State Mater. Sci.* **1998**, *3*, 159−167.
(2) Yeon, J.; Smith, M. D.; Tapp, J.; Möller, A.; zur Loye, H.-C. *J. Am. Chem. Soc.* **2014**, *136*, 3955−3963.
(3) Kim, S. W.; Kim, S.-H.; Halasyamani, P. S.; Green, M. A.; Bhatti, K. P.; Leighton, C.; Das, H.; Fennie, C. J. *Chem. Sci.* **2012**, *3*, 741−751.
(4) Yeon, J.; Smith, M. D.; Tapp, J.; Möller, A.; zur Loye, H.-C. *Inorg. Chem.* **2014**, *53*, 6289−6298.
(5) Abeysinghe, D.; Smith, M. D.; Yeon, J.; Morrison, G.; zur Loye, H.-C. *Cryst. Growth Des.* **2014**, *14*, 4749−4758.
(6) Cortese, A. J.; Wilkins, B.; Smith, M. D.; Yeon, J.; Morrison, G.; Tran, T. T.; Halasyamani, P. S.; zur Loye, H.-C. *Inorg. Chem.* **2015**, *54*, 4011−4020.
(7) Chance, W. M.; Bugaris, D. E.; Sefat, A. S.; zur Loye, H.-C. *Inorg. Chem.* **2013**, *52*, 11723−11733.
(8) Latshaw, A. M.; Chance, W. M.; Trenor, N.; Morrison, G.; Smith, M. D.; Yeon, J.; Williams, D. E.; zur Loye, H.-C. *CrystEngComm* **2015**, *17*, 4691−4698.
(9) Bugaris, D. E.; Smith, M. D.; zur Loye, H.-C. *Inorg. Chem.* **2013**, *52*, 3836−3844.
(10) Liao, C.-H.; Chang, P.-C.; Kao, H.-M.; Lii, K.-H. *Inorg. Chem.* **2005**, *44*, 9335−9339.
(11) Tang, M.-F.; Chiang, P.-Y.; Su, Y.-H.; Jung, Y.-C.; Hou, G.-Y.; Chang, B.-C.; Lii, K.-H. *Inorg. Chem.* **2008**, *47*, 8985−8989.
(12) Yu, H.; Wu, H.; Pan, S.; Wang, Y.; Yang, Z.; Su, X. *Inorg. Chem.* **2013**, *52*, 5359−5365.
(13) Huang, Q.; Hwu, S.-J. *Inorg. Chem.* **2003**, *42*, 655−657.
(14) West, J. P.; Hwu, S.-J. *J. Solid State Chem.* **2012**, *195*, 101−107.
(15) Queen, W. L.; West, J. P.; Hwu, S.-J.; VanDerveer, D. G.; Zarzyczny, M. C.; Pavlick, R. A. *Angew. Chem., Int. Ed.* **2008**, *47*, 3791−3794.
(16) Barrer, R. M.; Meier, W. M. *J. Chem. Soc.* **1958**, 299−304.
(17) Jaeger, F. M. *Trans. Faraday Soc.* **1929**, *25*, 320−345.
(18) Huang, Q.; Ulutagay, M.; Michener, P. A.; Hwu, S.-J. *J. Am. Chem. Soc.* **1999**, *121*, 10323−10326.
(19) Hwu, S.-J.; Ulutagay-Kartin, M.; Clayhold, J. A.; Mackay, R.; Wardojo, T. A.; O'Connor, C. J.; Krawiec, M. *J. Am. Chem. Soc.* **2002**, *124*, 12404−12405.
(20) Rabinowitch, E.; Belford, R. L. *Spectroscopy and Photochemistry of Uranyl Compounds*; Macmillan: New York, 1964.
(21) Morrison, G.; Tran, T. T.; Halasyamani, P. S.; zur Loye, H.-C. *Inorg. Chem.* **2016**, *55*, 3215−3217.
(22) Read, C. M.; Yeon, J.; Smith, M. D.; zur Loye, H.-C. *CrystEngComm* **2014**, *16*, 7259−7267.
(23) Read, C. M.; Smith, M.; zur Loye, H.-C. *J. Chem. Crystallogr.* **2015**, *45*, 440−444.
(24) Ulutagay, M.; Schimek, G. L.; Hwu, S.-J.; Taye, H. *Inorg. Chem.* **1998**, *37*, 1507−1512.
(25) Huang, Q.; Hwu, S.-J.; Mo, X. *Angew. Chem., Int. Ed.* **2001**, *40*, 1690−1693.
(26) Stern, R.; Heinmaa, I.; Kriisa, A.; Joon, E.; Vija, S.; Clayhold, J.; Ulutagay-Kartin, M.; Mo, X.; Queen, W.; Hwu, S. J. *Phys. B* **2006**, *378*−*380*, 1124−1125.
(27) Morrison, G.; zur Loye, H.-C. *Cryst. Growth Des.* **2016**, *16*, 1294−1299.
(28) Lee, C.-S.; Wang, S.-L.; Chen, Y.-H.; Lii, K.-H. *Inorg. Chem.* **2009**, *48*, 8357−8361.
(29) Kahlenberg, V.; Manninger, T. *Acta Crystallogr., Sect. E: Struct. Rep. Online* **2014**, *70*, i11.
(30) Lin, X.; Zhang, F.; Pan, S.; Yu, H.; Zhang, F.; Dong, X.; Han, S.; Dong, L.; Bai, C.; Wang, Z. *J. Mater. Chem. C* **2014**, *2*, 4257−4264.
(31) Choudhury, A.; Dorhout, P. K. *Inorg. Chem.* **2006**, *45*, 5245−5247.
(32) Chang, Y.-C.; Chang, W.-J.; Boudin, S.; Lii, K.-H. *Inorg. Chem.* **2013**, *52*, 7230−7235.
(33) Yeon, J.; Felder, J. B.; Smith, M. D.; Morrison, G.; zur Loye, H.-C. *CrystEngComm* **2015**, *17*, 8428−8440.
(34) Wang, Z.; Zachara, J. M.; Gassman, P. L.; Liu, C.; Qafoku, O.; Yantasee, W.; Catalano, J. G. *Geochim. Cosmochim. Acta* **2005**, *69*, 1391−1403.
(35) Jackson, J. M.; Burns, P. C. *Can. Mineral.* **2001**, *39*, 187−195.
(36) Wronkiewicz, D. J.; Bates, J. K.; Wolf, S. F.; Buck, E. C. *J. Nucl. Mater.* **1996**, *238*, 78−95.
(37) Ewing, R. C. *Can. Mineral.* **2001**, *39*, 697−715.
(38) Council, N. R. *Glass as a Waste Form and Vitrification Technology: Summary of an International Workshop*; The National Academies Press: Washington, D.C., 1996.
(39) Wang, S.; Alekseev, E. V.; Ling, J.; Skanthakumar, S.; Soderholm, L.; Depmeier, W.; Albrecht-Schmitt, T. E. *Angew. Chem., Int. Ed.* **2010**, *49*, 1263−1266.
(40) Gauld, I. C.; Giaquinto, J. M.; Delashmitt, J. S.; Hu, J.; Ilas, G.; Haverlock, T. J.; Romano, C. *Ann. Nucl. Energy* **2016**, *87*, 267−281.
(41) Morrison, G.; Read, C. M.; Smith, M. D.; zur Loye, H.-C. *CrystEngComm* **2015**, *17*, 1968−1974.
(42) Nazarchuk, E. V.; Siidra, O. I.; Zadoya, A. I.; Agakhanov, A. A. *Inorg. Chem. Commun.* **2015**, *62*, 15−18.
(43) *SAINT+*, v. 6.0; Bruker Analytical X-ray Systems: Madison, Wisconsin, USA, 2000.
(44) *SADABS*, v. 2.03; Bruker Analytical X-ray Systems: Madison, Wisconsin, USA, 2002.
(45) Sheldrick, G. *Acta Crystallogr., Sect. A: Found. Adv.* **2015**, *71*, 3−8.
(46) Hubschle, C. B.; Sheldrick, G. M.; Dittrich, B. *J. Appl. Crystallogr.* **2011**, *44*, 1281−1284.
(47) Dolomanov, O. V.; Bourhis, L. J.; Gildea, R. J.; Howard, J. A. K.; Puschmann, H. *J. Appl. Crystallogr.* **2009**, *42*, 339−341.
(48) Farrugia, L. *J. Appl. Crystallogr.* **1999**, *32*, 837−838.
(49) Bugaris, D. E.; zur Loye, H.-C. *Angew. Chem., Int. Ed.* **2012**, *51*, 3780−3811.
(50) Burns, P. C. *Rev. Mineral. Geochem.* **1999**, *38*, 23−90.
(51) Liebau, F. *Structural Chemistry of Silicates: Structure, Bonding, and Classification*; Springer-Verlag: New York, 1985.
(52) Brown, I. D.; Altermatt, D. *Acta Crystallogr., Sect. B: Struct. Sci.* **1985**, *41*, 244−247.
(53) Burns, P. C.; Ewing, R. C.; Hawthorne, F. C. *Can. Mineral.* **1997**, *35*, 1551−1570.
(54) Balboni, E.; Burns, P. C. *J. Solid State Chem.* **2014**, *213*, 1−8.
(55) *CRC Handbook of Chemistry and Physics*, 86th ed.; Lide, D. R., Ed.; Taylor & Francis: New York, 2005.
(56) Leinenweber, K.; Johnson Jennifer, E.; Groy Thomas, L. *Am. Mineral.* **2005**, *90*, 115.
(57) Shannon, R. *Acta Crystallogr., Sect. A: Cryst. Phys., Diffr., Theor. Gen. Crystallogr.* **1976**, *32*, 751−767.
(58) Voss, N. R.; Gerstein, M. *Nucleic Acids Res.* **2010**, *38*, W555−W562.
(59) The volume of a Cs^+ is calculated based on the Shannon's crystal radius. The volume of Cs_6F was calculated using the volume assessor in the ^{3}V program. A PDB file was created containing a cluster with angles and distances typical Cs_6F. However, since the volume assessor uses the Van der Waals radii of the atoms, all Cs atoms where replaced by P atoms (Shannon's crystal radius of Cs^+ is approximately equal to the Van der Waals radii of P). To determine the volume, this cluster was scanned using a probe with a comparable radius to that of an oxygen (based on the Shannon's crystal radius).
(60) Baird, C. P.; Kemp, T. J. *Prog. React. Kinet.* **1997**, *22*, 87−139.
(61) Spek, A. L. *J. Appl. Crystallogr.* **2003**, *36*, 7−13.

DOI: 10.1021/jacs.6b03205
J. Am. Chem. Soc. 2016, 138, 7121−7129